metals

Article

The Effect of the Si Content on the Morphology and Amount of Fe_2SiO_4 in Low Carbon Steels

Qing Yuan, Guang Xu *, Mingxing Zhou and Bei He

The State Key Laboratory of Refractories and Metallurgy, Hubei Collaborative Innovation Center for Advanced Steels, Wuhan University of Science and Technology, 947 Heping Avenue, Qingshan District, Wuhan 430081, China; 15994235997@163.com (Q.Y.); kdmingxing@163.com (M.Z.); 15071412662@163.com (B.H.)
* Correspondence: xuguang@wust.edu.cn; Tel.: +86-156-9718-0996; Fax: +86-27-6886-2807

Academic Editors: Vineet V. Joshi and Alan Meier
Received: 3 March 2016; Accepted: 12 April 2016; Published: 22 April 2016

Abstract: In order to study the effect of the Si content on the morphology, amount, and distribution of fayalite (Fe_2SiO_4), three low-carbon steels with different Si contents were selected, and reheating tests were conducted in an industrial furnace in a hot strip plant. The results show that Si distributes in two forms—first, Fe_2SiO_4, in the innermost layer of the oxide scale, and, second, granular SiO_2, dispersively distributed in the matrix near the scale. In addition, Fe_2SiO_4 appears in a net-like form in the innermost layer of the oxide scale close to the iron matrix when the Si content is 1.21 wt. %. However, no obvious net-like Fe_2SiO_4 is observed when the Si content is less than 0.25 wt. %. Moreover, the inhibition effect of the solid Fe_2SiO_4 on the oxidation reaction plays a more important role than the promotion effect of the liquid Fe_2SiO_4 during the entire oxidation reaction. Therefore, the total thickness of the scale decreases with the increase in Si content.

Keywords: Si content; oxide scale; Fe_2SiO_4; X-ray diffraction

1. Introduction

Silicon is generally added to steels as one of the solid solution-strengthening elements [1]. The surface defects, such as rolled-in scale, red scale, and chromatic aberration, appear in hot-rolled low-carbon steels containing silicon [2,3]. The existing research shows that the red scale has a close relationship with the silicon element in steel [4–7]. So far, some studies have been conducted on the red scale. Suarez *et al.* [8] investigated the influence of silicon on the formation of the oxide scale in hot-rolled strips at high temperatures. They pointed out that Si reacts with oxygen diffusing into steel and precipitates as SiO_2, which combines with FeO and forms a separate phase called fayalite (Fe_2SiO_4). The melting point of Fe_2SiO_4 is about 1173 °C. Fe_2SiO_4 begins to form at a temperature above 750 °C and primarily aggregates on the interface between the iron matrix and the scale. Fukaga *et al.* [9] and Onoda *et al.* [10] analyzed the relationship between the Fe_2SiO_4 phase and the red scale. They claimed that the oxide layer formed on the steel surface mainly consists of Fe_2O_3, Fe_3O_4, and FeO. The eutectic FeO/Fe_2SiO_4 primarily forms in the interface between the matrix and the scale, and irregularly penetrates into FeO and the matrix. It is difficult to absolutely wipe off the FeO layer after descaling due to the very high strength of the eutectic compound. The remaining FeO scale is oxidized into red Fe_2O_3 during the following cooling process. Furthermore, the descaling process becomes more difficult and more red scale remains when the penetrative depth of the Fe_2SiO_4 phase in the FeO layer is larger. In addition, only a few studies have been conducted about the effect of the Si element on the content of Fe_2SiO_4 in low-carbon steel. Schneider *et al.* [8] investigated the oxidation of Fe-Si alloys at high temperatures from 900 to 1250 °C, and found that the amount of Fe_2SiO_4 and the thickness of the scale increase with the silicon content. In addition, the liquid Fe_2SiO_4 accelerated the oxidation process. Moreover, Mouayd *et al.* [11] reported that the penetrative depth of the eutectic FeO/Fe_2SiO_4 in the scale increases with Si content.

It is generally accepted that the formation of the red scale is related not only to the content of Fe_2SiO_4, but also to its morphology and distribution. However, almost all existing studies were performed in laboratories, and oxidizing atmosphere was not added until isothermal holding temperature. Moreover, the effect of Si content on the morphology and quantitative studies on the amount of Fe_2SiO_4 has scarcely been reported. In the present study, three low-carbon steels with different Si contents were selected, and reheating tests were conducted in an industrial furnace in a hot strip plant to quantitatively study the effect of the silicon content on the morphology and amount of Fe_2SiO_4. The novelty in the present study is that a new influence rule of silicon on the oxidation behavior in Si-containing steel has been proposed. In addition, oxidation tests were first conducted with the same atmosphere and heating route as industrial heating technology.

2. Materials and Methods

2.1. Oxidation Experiment and Sample Preparation

Three low-carbon steels were commercially produced in a hot strip plant. All samples were formed in a cube-shaped structure of 133 mm × 39 mm × 10 mm. The samples were polished to remove the scale before heating in the furnace. The chemical compositions of the three carbon steels with different Si contents are presented in Table 1. The heating procedure is shown in Figure 1. The samples were heated to 1260 °C by segment heating route and held for 40 min, followed by air cooling to room temperature. The heating atmosphere in the furnace contained approximately 2% oxygen, 13% carbon dioxide, 11% water vapor, and 74% nitrogen. After oxidation experiment, specimens were cut using a wire-electrode cutting device. Since the oxide scale in these samples is very brittle and easy to peel off, the cold mounting method was used in the preparation of the samples for microscopic observation. The cold mounting material is composed of 60% acrylic powder and 40% liquid hardener. The cross-sections of mounted samples were grinded and polished. The powder was scraped off from samples without cold mounting for phase analysis via X-ray diffraction (XRD, Panalytical, Almelo, The Netherlands).

Table 1. The chemical compositions in tested steels (wt. %).

Steel	C	Si	Mn	P	S	Al	Fe
1	0.069	1.21	1.40	0.010	0.001	0.035	Balance
2	0.071	0.25	1.37	0.011	0.001	0.031	Balance
3	0.073	0.09	1.44	0.012	0.002	0.029	Balance

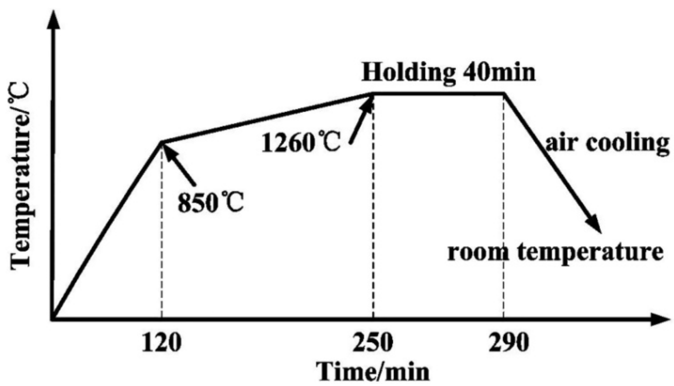

Figure 1. The heating procedure.

2.2. Oxide Scale Analyses

Three techniques were used to analyze the constitution of the oxide scale, *i.e.* a backscattered electron detection (BSED, FEI, Hillsboro, OR, USA), energy-dispersive spectroscopy (EDS, OIMS, Oxford, UK), and XRD. The microstructure and compositions of the oxide scale were analyzed via BSED and EDS on a Nova 400 Nano scanning electron microscope (SEM, FEI, Hillsboro, OR, USA) operated at an accelerating voltage of 20 kV. XRD with Cu Kα radiation was also used to analyze the phase of the oxide scale under the following conditions: acceleration voltage, 40 kV; current, 150 mA; step, 0.06°. The powder sample for XRD was scraped from the oxidized sample. Furthermore, the Image-Pro plus 6.0 software (Media Cybernetics, Rockville, MD, USA) was used to determine the total thickness of the scale and the Fe_2SiO_4 layer.

3. Results and Discussions

3.1. Morphology and the Composition of the Oxide Scale

The morphological images of the oxide scale in three low-carbon steels are shown in Figure 2. It can be seen that the oxide scale consists of three layers with different thicknesses. According to the latter results of EDS and XRD, the upper layer primarily contains Fe_2O_3. The middle layer is thicker compared to the upper layer and consists of FeO and Fe_3O_4 (Figure 2a,c,e). The inner layer is a mixture of Fe_2SiO_4 and FeO. The dark gray Fe_2SiO_4 distributes in the light gray FeO. Fe_2SiO_4 appears in the net-like form when the silicon content is high (Figure 2b). However, no obvious net-like Fe_2SiO_4 is observed when the Si content is low (Figure 2f).

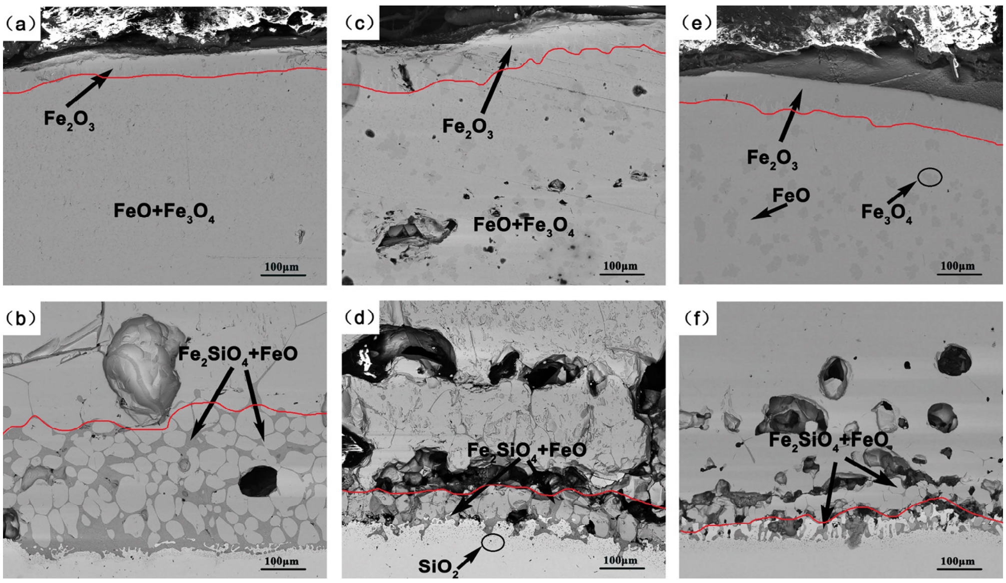

Figure 2. The morphology micrographs of oxide scale on cross-sections of three steels. (**a**) The upper and middle layers and (**b**) the inner layer of Steel 1 (Si 1.21%); (**c**) the upper and middle layers and (**d**) the inner layer of Steel 2 (Si 0.25%); (**e**) the upper and middle layers and (**f**) the inner layer of Steel 3 (Si 0.09%).

The thickness of the upper layer in all three carbon steels is thinner compared to other layers. Some dispersive dark spots, confirmed to be Fe_3O_4 as determined by EDS, can be observed in the middle layer (Figure 2a,c,e). In addition, small dark spots are dispersively distributed in the matrix near the scale, and, according to the EDS results, these spots are confirmed to be SiO_2 (Figure 2b,d,f). Fe_2SiO_4 appears in the net-like form in Steel 1 containing higher silicon content (Figure 2b), whereas no obvious net-like Fe_2SiO_4 is observed in Steels 2 and 3 with low Si content (Figure 2d,f). According to the distribution of Fe_2SiO_4 in Figure 2, the amount of Fe_2SiO_4 decreases with the reduction in the silicon content. In Steels 2 and 3 with low silicon content, the penetration of Fe_2SiO_4 along the grain boundary is less because of a small amount of Fe_2SiO_4, leading to unnoticeable net-like Fe_2SiO_4. In Steel 1 with 1.21 wt. % silicon, the net-like Fe_2SiO_4 can be easily observed in the innermost layer of the oxide scale close to the iron matrix.

EDS and XRD were applied to determine the phases in each layer of the oxide scale. Figure 3 shows the EDS results of the scale in Steel 1 and indicates that each layer of the scale not only contains Fe and O elements, but also includes Mn. Moreover, silicon is detected in the innermost layer of the scale (Figure 3c), indicating that a silicon-enriched phase forms in this layer. Table 2 provides the atomic percentage of the main elements of each layer of the scale in Steel 1. It can be seen that the oxygen content gradually decreases from the upper layer to the inner layer. Moreover, the content of the Mn element increases from outside to inside of the scale as a result of Mn diffusion [12]. The single oxide of Mn is not detected in the oxide layers.

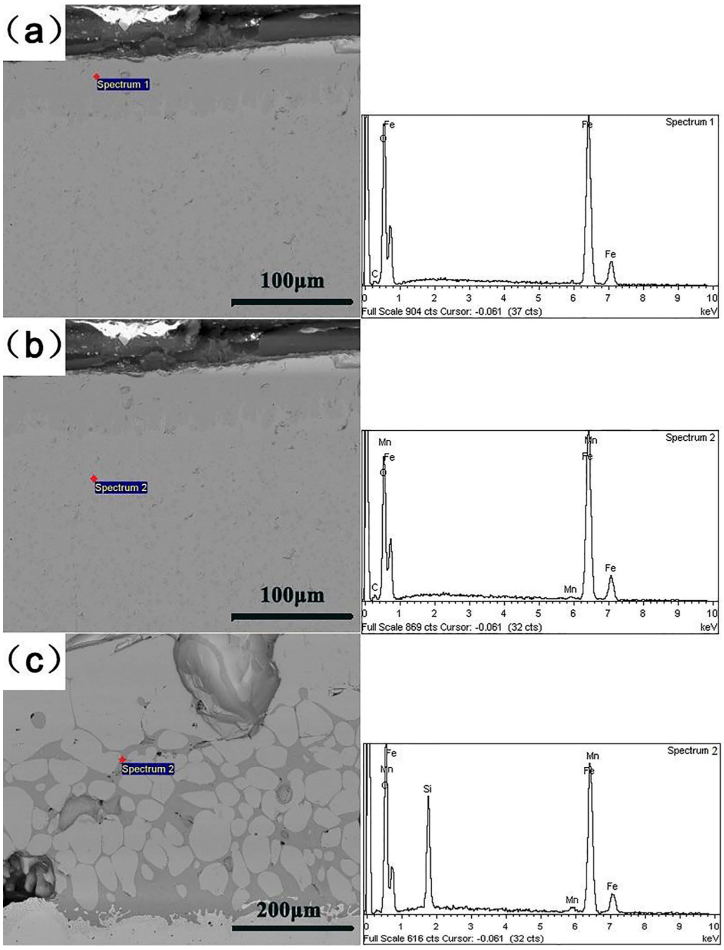

Figure 3. Energy-dispersive spectroscopy (EDS) results of oxide scale for Steel 1. (**a**) Upper layer; (**b**) middle layer; (**c**) inner layer.

Table 2. The main atomic percentage of each layer in sample Steel 1 (atom %).

Chemical Elements		O	Si	Fe	Mn
Inner layer	dark area	54.20	12.85	32.0	0.95
	bright area	54.63	-	44.54	0.83
Middle layer		55.86	-	43.50	0.64
Upper layer		57.65	-	41.77	0.58

The atomic ratios of the oxide in each layer can be calculated according to Table 2. The atomic ratios of Fe/O in the outermost and middle layers are approximately 2/3 and 1/1, respectively. The atomic ratio of Fe/Si/O in the inner layer is about 2/1/4. The corresponding XRD results of the scale in Steel 1 are shown in Figure 4, in which no silicon is detected because it is difficult to scrape the inner layer scale containing silicon from the matrix surface. The phase of each layer can be determined by combining the EDS and XRD results. The upper layer contains Fe_2O_3, and the middle layer consists of FeO, and a small amount of Fe_3O_4. According to the EDS results in Table 2, the inner layer is a composite of eutectic compounds Fe_2SiO_4/FeO. The dark area is mainly Fe_2SiO_4, while the bright area is FeO. The constitution of oxide layers is consistent with the results in the other studies [2,9].

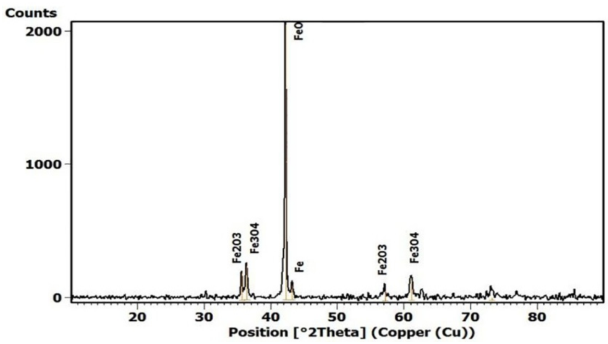

Figure 4. X-ray diffraction (XRD) results of oxide scale for Steel 1.

3.2. Penetrative Depth of Fe_2SiO_4 and the Total Thickness of the Scale

The Image-Pro plus 6.0, an image-processing software, was used to measure the areas of Fe_2SiO_4 in unit width. First, the total areas of Fe_2SiO_4 in inner layers were measured by the color aberration with software. Then, the total areas were divided by the width of measured images to obtain the areas of Fe_2SiO_4 in unit width. Several images were used to improve the accuracy of the Fe_2SiO_4 measurement. The measured area can represent the amount of Fe_2SiO_4, and the results are presented in Figure 5. It can be seen that the amount of the silicon-enriched phase Fe_2SiO_4 decreases with the reduction in the silicon content. The decreased amount of Fe_2SiO_4 weakens its anchor effect [10] to scale, which helps to prevent the red scale.

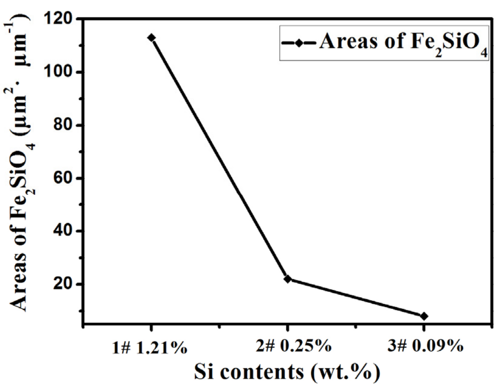

Figure 5. The areas of Fe_2SiO_4 in three tested steels.

Figure 6 shows the relationships between the silicon content, the penetrative depth of Fe_2SiO_4, and the total thickness of the scale. It is indicated from curve "a" that the penetrative depth of Fe_2SiO_4 increases with the silicon content. The Pilling-Bedworth ratio (PBR) of Fe oxide or Si oxide is more than 1 at a temperature of 1260 °C [13]. PBR is the ratio of the oxide volume and the consumed metal volume. The PBR is greater than 1 because the volume of oxide is larger than that of the consumed metal, leading to a compressive stress in the oxide [14]. In other words, during the oxidation process, the oxidized part of the metal expands compared with the metal and the compressive stress is produced in the oxide scale. Moreover, the compressive stress at the layer/metal interface is larger than that at the outer position, leading to the pressure difference in different places of the scale. The pressure difference in the liquefied Fe_2SiO_4 phase at a temperature of 1260 °C compels a part of Fe_2SiO_4 to permeate into the inner scale. The liquid Fe_2SiO_4 phase distributes along the FeO grain boundary and the net-like Fe_2SiO_4 phase forms after its solidification. A larger compressive stress due to more Fe_2SiO_4 in steels with a higher silicon content results in a deeper penetration layer. Furthermore, the above theory can also be used to explain the morphological change of Fe_2SiO_4 with silicon contents.

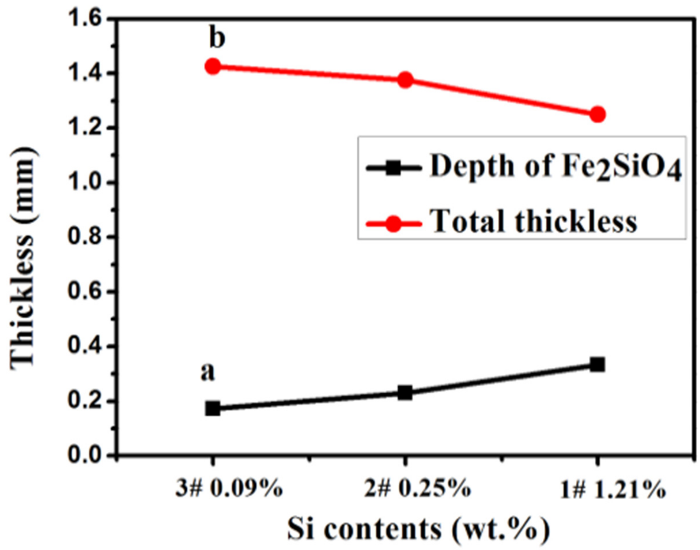

Figure 6. The penetrative depth of fayalite (Fe_2SiO_4) and total scale thickness in three different silicon-content steels.

Curve "b" in Figure 6 indicates that the total thickness of the scale decreases with the increase in the silicon content during industrial reheating test. The solid-state Fe_2SiO_4 at the stage of low temperature below the melting temperature of Fe_2SiO_4 (1173 °C) acts as an ion diffusion barrier to prevent further formation of iron oxide. The solid Fe_2SiO_4 increases with the silicon content, thus the inhibition effect is enhanced and the total thickness of the scale decreases with the increase in the silicon content. However, Li *et al.* [15] claimed that the total thickness of the scale increases with the silicon content. They explained that the liquefied FeO/Fe_2SiO_4 provides fast diffusion passages for the ions at 1200 °C and it is an important factor for a sharp increase in the thickness of the scale with the silicon content. Similar results were reported by Mouayd *et al.* [11]. The results of this study are different from theirs. This is because Fe_2SiO_4 has two opposite effects on the oxidation of steels, *i.e.*, the solid Fe_2SiO_4 hinders oxidation and the liquid Fe_2SiO_4 promotes oxidation. In their experiments, the oxidizing atmosphere was pumped in at a temperature higher than the melting temperature of Fe_2SiO_4 (1173 °C). Therefore, only the promotion effect of Fe_2SiO_4 was presented and the total thickness of the scale increased with the Si content. However, the experimental procedures in their studies were not suitable for the industrial reheating scenario. In the present study, industrial experiments were conducted and the oxidizing atmosphere was pumped in from the beginning of the test. The solid-state Fe_2SiO_4 hindered the oxidation reaction at a lower temperature, whereas the liquefied Fe_2SiO_4 accelerated it when the temperature was higher than the melting temperature of Fe_2SiO_4 (1173 °C). However, the total thickness of the scale decreased with the increase of the silicon content. The decrease in the total thickness of the scale is attributed to the inhibition effects of Fe_2SiO_4. It indicates that the inhibition effect of Fe_2SiO_4 on the oxidation reaction plays a more important role during the entire oxidation reaction.

3.3. Distribution of Silicon

Line scanning and area scanning for Steel 1 with more silicon were applied to observe the distribution of silicon in the scale and the iron matrix near the scale. Figure 7 presents the results of the Si distribution in the scale by line scanning and area scanning. As shown in Figure 7b, silicon primarily concentrates at the inner scale. Meanwhile, as shown in Figure 7c, a sudden increase in the silicon content indicates that a silicon-enriched phase was formed in the inner scale.

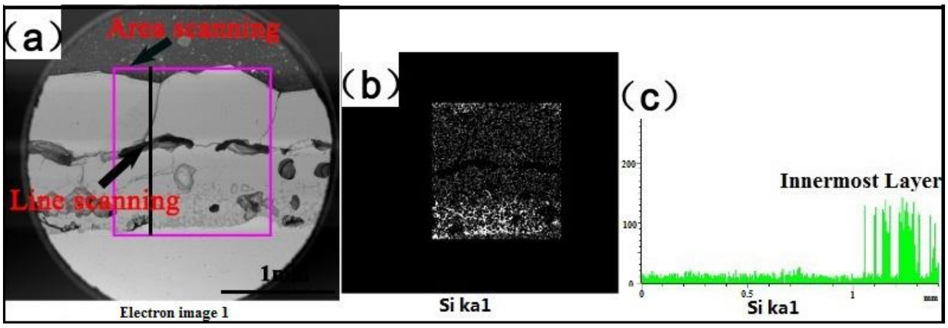

Figure 7. The results of Si distribution in inner scale by line scanning and area scanning. (**a**) The morphology micrographs of oxide scale; (**b**) the results of area scanning; (**c**) the results of line scanning.

The results of the Si distribution in the iron matrix near the scale are presented in Figure 8. According to the results of the energy spectrum in Figure 8c, combined with references [4,5], the dark spots may be classified as silicon dioxide. Figure 9 shows the schematic diagram that explains the formation of the granular silicon dioxide in the iron matrix near the interface. As shown in the diagram, for Si-containing steels, an outer iron oxide layer is initially formed under the oxidizing atmosphere. However, many cracks and holes may exist in the iron oxide thus formed, and these cracks and holes turn out to be the passage by which oxygen permeates into the iron matrix. When the concentration of oxygen is very high, the chemical reaction of Si and O_2 takes place to form SiO_2 in the iron matrix. A part of SiO_2 combines with FeO to form Fe_2SiO_4, whereas others remain in the iron matrix. Therefore, silicon primarily concentrates in Fe_2SiO_4 in the inner scale and SiO_2 particles in the iron matrix near the scale.

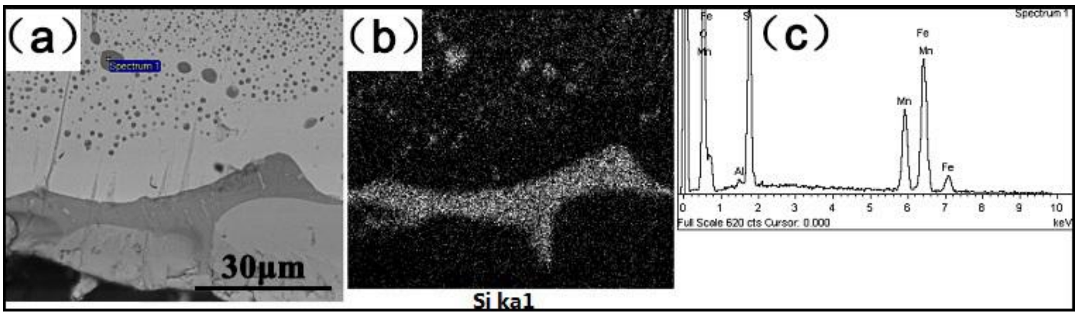

Figure 8. The results of Si distribution in iron matrix near scale by area scanning and energy spectrum. (**a**) The distribution of Si-containing scale and particles; (**b**) the results of area scanning; (**c**) the results of EDS.

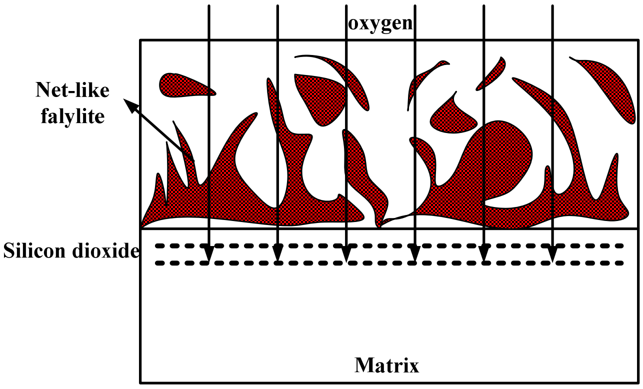

Figure 9. The schematic diagram of the formation of granular silicon dioxide in iron matrix.

4. Conclusions

In this study, three low-carbon steels with different Si contents were selected, and reheating tests were conducted in an industrial furnace in a hot strip plant. The effect of the Si content on the morphology, amount, and distribution of Fe_2SiO_4 was quantitatively analyzed via backscattered electron detection (BSED), energy-dispersive spectroscopy (EDS), and X-ray diffraction (XRD). The results show that Si distributes in two forms, *i.e.* Fe_2SiO_4, in the innermost layer of the oxide scale, and granular SiO_2, dispersively distributed in the matrix near the scale. In addition, Fe_2SiO_4 appears in the net-like form in the innermost layer of the oxide scale close to the iron matrix when the Si content is 1.21 wt. %. However, no obvious net-like Fe_2SiO_4 is observed when the Si content is less than 0.25 wt. %. Moreover, the inhibition effect of the solid Fe_2SiO_4 on the oxidation reaction plays a more important role than the promotion effect of the liquid Fe_2SiO_4 during the entire oxidation reaction. Therefore, the total thickness of the scale decreases with the increase in Si content.

Acknowledgments: The authors gratefully acknowledge the financial supports from the National Natural Science Foundation of China (NSFC) (No. 51274154), the State Key Laboratory of Development and Application Technology of Automotive Steels (Baosteel Group).

Author Contributions: Guang Xu conceived and designed the experiments; Qing Yuan conducted experiments, analyzed the data, and wrote the paper; Mingxing Zhou conducted experiments; Bei He conducted experiments.

Conflicts of Interest: The authors declare no conflict of interest. The founding sponsors had no role in the design of the study; in the collection, analyses, or interpretation of data; in the writing of the manuscript; or in the decision to publish the results.

References

1. Hu, J.; Du, L.X.; Wang, J.J.; Gao, C.R.; Yang, T.Z.; Wang, A.Y.; Misra, R.D.K. Microstructures and Mechanical Properties of a New As-Hot-Rolled High-Strength DP Steel Subjected to Different Cooling Schedules. *Metall. Mater. Trans. A* **2013**, *44*, 4937–4947. [CrossRef]
2. Okada, H.; Fukagawa, T.; Ishihara, H.; Okamoto, A.; Azuma, M.; Matsuda, Y. Effects of hot-rolling and descaling condition on red scale defects formation. *ISIJ Int.* **1994**, *80*, 849–854.
3. Chattonpadhyay, A.; Chanda, T. Role of silicon on oxide morphology and pickling behavior of automotive steels. *Scr. Mater.* **2008**, *58*, 882–885. [CrossRef]
4. Liu, X.J.; Cao, G.M.; He, Y.Q.; Jia, T.; Liu, Z.Y. Effect of temperature on scale morphology of Fe-1.5Si alloy. *J. Iron Steel Res. Int.* **2013**, *20*, 73–78. [CrossRef]
5. Yang, Y.L.; Yang, C.H.; Lin, S.N.; Chen, C.H.; Tsai, W.T. Effects of Si and its content on the scale formation on hot-rolled steel strips. *Mater. Chem. Phys.* **2008**, *112*, 566–571. [CrossRef]
6. Cao, G.M.; Liu, X.J.; Sun, B.; Liu, Z.Y. Morphology of Oxide Scale and Oxidation Kinetics of Low Carbon Steel. *J. Iron Steel Res. Int.* **2014**, *21*, 335–341. [CrossRef]
7. Kusabiraki, K.; Watanabe, R.; Ikehata, T. High-temperature oxidation behavior and scale morphology of Si-containing steels. *ISIJ Int.* **2007**, *47*, 1329–1334. [CrossRef]

8. Suarez, L.; Schneider, J.; Houbaert, Y. High-temperature oxidation of Fe-Si alloys in the temperature range 900–1250 °C. *Defect Diffus. Forum* **2008**, *273–276*, 661–666. [CrossRef]
9. Okada, H.; Fukagawa, T.; Ishihara, H. Prevention of red scale formation during hot rolling of steels. *ISIJ Int.* **1995**, *35*, 886–891. [CrossRef]
10. Fukagawa, T.; Okada, H.; Maeharara, Y. Mechanical of red scale defect formation in Si-added hot-rolled steels. *ISIJ Int.* **1994**, *34*, 906–911. [CrossRef]
11. Mouayd, A.A.; Koltsov, A.; Sutter, E.; Tribollet, B. Effect of silicon content in steel and oxidation temperature on scale growth and morphology. *Mater. Chem. Phys.* **2014**, *143*, 996–1004. [CrossRef]
12. Zhang, Y.S.; Rapp, R.A. Solubilities of CeO_2, HfO_2 and Y_2O_3 in Fused Na_2SO_4-30 mol % $NaVO_3$ and CeO_2 in Pure Na_2SO_4 at 900 °C. *Corrosion* **1987**, *43*, 348–352. [CrossRef]
13. Staettle, R.W.; Fontana, M.G. *Advances in Corrosion Science and Technology*; Springer-Verlag: New York, NY, USA, 1974; pp. 239–356.
14. Garnaud, G.; Rapp, R.A. Thickness of the oxide layers formed during the oxidation of iron. *Oxid. Met.* **1977**, *11*, 193–198. [CrossRef]
15. Li, S.J.; Liu, Y.B.; Zhang, W.; Sun, Q.S.; Wang, L.P. Effects of silicon on spring steel oxidation rate under 2% residual oxygen atmosphere. *J. Iron Steel Res. Int.* **2015**, *55*, 27–60. (In Chinese)

© 2016 by the authors; licensee MDPI, Basel, Switzerland. This article is an open access article distributed under the terms and conditions of the Creative Commons Attribution (CC-BY) license (http://creativecommons.org/licenses/by/4.0/).